Characterization of 4H–SiC substrates and epilayers by Fourier transform infrared reflectance spectroscopy*

Dong Lin(董 林)[a)†], Sun Guo-Sheng(孙国胜)[a)b)c)], Zheng Liu(郑 柳)[a)], Liu Xing-Fang(刘兴昉)[a)], Zhang Feng(张 峰)[a)], Yan Guo-Guo(闫果果)[a)], Zhao Wan-Shun(赵万顺)[a)], Wang Lei(王 雷)[a)], Li Xi-Guang(李锡光)[c)], and Wang Zhan-Guo(王占国)[b)]

[a)] *Material Science Center, Institute of Semiconductors, Chinese Academy of Sciences, Beijing* 100083, *China*

[b)] *Key Laboratory of Semiconductor Material Sciences, Institute of Semiconductors, Chinese Academy of Sciences, Beijing* 100083, *China*

[c)] *Dongguan Tianyu Semiconductor Inc., Dongguan* 523000, *China*

(Received 16 August 2011; revised manuscript received 11 October 2011)

The infrared reflectance spectra of both 4H–SiC substrates and epilayers are measured in a wave number range from 400 cm^{-1} to 4000 cm^{-1} using a Fourier-transform spectrometer. The thicknesses of the 4H–SiC epilayers and the electrical properties, including the free-carrier concentrations and the mobilities of both the 4H–SiC substrates and the epilayers, are characterized through full line-shape fitting analyses. The correlations of the theoretical spectral profiles with the 4H–SiC electrical properties in the 30 cm^{-1}–4000 cm^{-1} and 400 cm^{-1}–4000 cm^{-1} spectral regions are established by introducing a parameter defined as error quadratic sum. It is indicated that their correlations become stronger at a higher carrier concentration and in a wider spectral region (30 cm^{-1}–4000 cm^{-1}). These results suggest that the infrared reflectance technique can be used to accurately determine the thicknesses of the epilayers and the carrier concentrations, and the mobilities of both lightly and heavily doped 4H–SiC wafers.

Keywords: 4H–SiC, infrared reflectance, epilayer thickness, electrical properties

PACS: 78.30.–j, 71.20.Nr **DOI:** 10.1088/1674-1056/21/4/047802

1. Introduction

Silicon carbide is a very promising semiconductor for high-power, high-temperature devices due to its wide band gap, high thermal conductivity, and high breakdown electric field.[1,2] High-quality 4H–SiC substrates and epilayers are especially required in 4H–SiC power device applications.[3] For the sake of examining the quality of 4H–SiC, conventional electrical characterization methods, such as capacitance–voltage (C–V) and Hall-effect measurements, have been widely used to determine the carrier concentration and mobility. Recently, optical techniques have proven to be effective alternative methods due to their nondestructive and contactless characteristics. For example, Raman scattering measurements could be used to simultaneously determine the carrier concentrations and mobilities of 4H–SiC and 6H–SiC, via fitting the profiles of the longitudinal-optical phonon-plasmon coupled (LOPC) mode.[4,5] However, Raman scattering measurements cannot provide information about epilayer thickness.

The infrared reflectance technique is another important optical approach to the characterization of SiC materials. Narita *et al.*[6] fitted the whole infrared spectrum of n-type 6H–SiC substrates to estimate carrier concentration and mobility, based on the modified classical dielectric function model. For SiC epilayers, a fitting analysis was also performed to calculate the epilayer thickness and the carrier concentration and mobility.[7] However, the fitting formulae were valid only in the case of normal incidence, and the correlations between the spectral profiles and electrical properties (i.e. carrier concentration and mobility) were not studied in detail because there were no appropriate parameters available to describe the correlations.

In this paper, we propose the fitting formulae of the infrared reflectance spectra for both the 4H–SiC substrates and epilayers. The thicknesses of the epilayers and the electrical properties of both 4H–SiC

*Project supported by the National Natural Science Foundation of China (Grand No. 60876003) and the Program of 2011 (2nd) Innovative Research Teams and Leading Talents in Guangdong Province of China.

†Corresponding author. E-mail: donglin09@semi.ac.cn

© 2012 Chinese Physical Society and IOP Publishing Ltd

substrates and epilayers are characterized by the fitting analyses of the infrared reflectance spectra. The values obtained by this method are compared with those obtained from the conventional measurements. Finally, the validity of the fitting technique is quantitatively discussed by introducing the error quadratic sum (EQS) parameter.

2. Experiment

A semi-insulating 4H–SiC substrate (Sample 1) and two heavily nitrogen-doped 4H–SiC substrates (Samples 2 and 3) with carrier concentrations of the order of 10^{18} cm^{-1} and 10^{19} cm^{-1}, respectively, were used in this work. A thick 4H–SiC homoepitaxial layer with a thickness of 14.4 μm was grown on an n^+ 4H–SiC substrate in a home-made vertical low pressure chemical vapour deposition (LPCVD) reactor. The thickness was determined by using cross-sectional scanning electron microscopy (SEM) (as shown in Fig. 1).

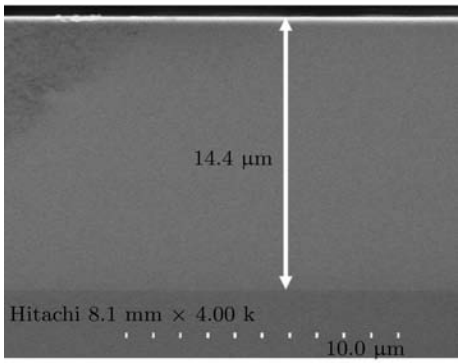


Fig. 1. Cross-sectional SEM image of a 4H–SiC epilayer.

The infrared reflectance spectra measurements were carried out at room temperature (RT) using a Spectrum GX Fourier-transform infrared (FTIR) spectrometer (Perkin Elmer Inc.) for the spectral region (400 cm^{-1}–4000 cm^{-1}) at an incident angle of 16°. A KBr beam splitter and a mid-IR deuterated triglycine sulfate (TGS) detector were used with a wave number resolution of 4 cm^{-1}. The polarization was unspecified both for incident and collected light. A silver mirror was used as a reference. The Hall-effect measurement was performed at RT to obtain the carrier concentrations and the mobilities of the substrates, and the Hall factor was assumed to be unity.[7] A mercury probe C–V measurement was performed at RT to obtain the carrier concentrations of the epilayers.

3. Theoretical analyses of infrared reflection spectra

3.1. Dielectric function model

Frequency-dependent dielectric function can be expressed as the sum of the lattice vibration term and the plasma oscillation term (i.e. the Drude term):[8]

$$\varepsilon_{\parallel,\perp}(\omega) = \varepsilon_{\infty}^{\parallel,\perp}\left(\frac{\omega_{\mathrm{L}\parallel,\perp}^2 - \omega^2 - \mathrm{i}\Gamma_{\mathrm{L}}\omega}{\omega_{\mathrm{T}\parallel,\perp}^2 - \omega^2 - \mathrm{i}\Gamma_{\mathrm{T}}\omega} - \frac{\omega_{\mathrm{p}\parallel,\perp}^2}{\omega(\omega+\mathrm{i}\gamma)}\right), \tag{1}$$

where $\varepsilon_{\parallel}$ and $\varepsilon_{\perp}$ are the dielectric functions in the directions parallel ($\parallel$) and perpendicular ($\perp$) to the c axis, respectively; ω is the wave number of the incident light; $\varepsilon_{\infty}^{\parallel,\perp}$ are the high-frequency dielectric constants; $\omega_{\mathrm{L}\parallel,\perp}$ and $\omega_{\mathrm{T}\parallel,\perp}$ are the longitudinal optical (LO) and transverse optical (TO) wave frequencies, respectively; Γ_{L} and Γ_{T} are the LO and TO wave damping constants, respectively; and $\omega_{\mathrm{p}\parallel,\perp}$ are the plasma frequencies, which are related to the concentration of the free carriers as

$$\omega_{\mathrm{p}\parallel,\perp} = \frac{1}{2\pi c}\sqrt{\frac{Nq^2}{m_{\parallel,\perp}^*\varepsilon_0\varepsilon_{\infty}^{\parallel,\perp}}}, \tag{2}$$

where N, q, $m_{\parallel,\perp}^*$, ε_0, and c are the free-carrier concentration, electron charge, electron effective mass, vacuum dielectric constant, and light velocity in vacuum, respectively. To simplify the following fitting calculations, only $\omega_{\mathrm{p}\perp}$ was chosen to be an adjustable parameter and $\omega_{\mathrm{p}\parallel}$ was set to be correlated with $\omega_{\mathrm{p}\perp}$, i.e. $\omega_{\mathrm{p}\parallel} = \sqrt{m_{\perp}^*\varepsilon_{\infty}^{\perp}/m_{\parallel}^*\varepsilon_{\infty}^{\parallel}}\omega_{\mathrm{p}\perp}$, according to Eq. (2); γ is the plasma damping constant, which is expressed as a function of carrier mobility, $\mu_{\parallel,\perp}$, as

$$\gamma = \frac{1}{2\pi c}\frac{q}{m_{\parallel,\perp}^*\mu_{\parallel,\perp}}. \tag{3}$$

It should be noted that Γ_{L}, Γ_{T}, and γ were assumed to be isotropic to reduce the complexity of the following fitting calculations. Equations (2) and (3) are the formulae from which we derived the carrier concentration and mobility. The values of $\mu_{\perp}$ were taken to compare with the Hall-effect measurement results.

3.2. Fitting formulae of infrared reflectance spectra

3.2.1. Substrate fitting

The fitting analyses for the SiC substrates have been performed by several groups.[6,8] However, their

fitting formulae are valid only in the case of normal incidence. Here we propose a fitting formula that is theoretically applicable to an arbitrary incident angle. The total reflectance $R_{\rm sub}$ can be expressed as a function of the reflectances of light polarized in the directions parallel (p) and perpendicular (s) to the incident plane:[9]

$$R_{\rm sub} = r^2_{\rm p,sub} \cdot \cos^2\alpha + r^2_{\rm s,sub} \cdot \sin^2\alpha, \tag{4}$$

where $r_{\rm p,sub}$ and $r_{\rm s,sub}$ are Fresnel reflection coefficients for p- and s-polarized light and depend on the dielectric function and incident angle;[10] and α is the angle included between the electric field vector of the incident wave and the plane of incidence. In the case of natural light, the intensities of p- and s-polarized light are equal, i.e. $\cos^2\alpha = \sin^2\alpha = 1/2$. Therefore $R_{\rm sub}$ becomes

$$R_{\rm sub} = (r^2_{\rm p,sub} + r^2_{\rm s,sub})/2. \tag{5}$$

3.2.2. Epilayer fitting

As the epilayer and substrate exhibit different forms of dielectric functions, the multi-reflection in the epilayer and the interference of the reflected light are required to be taken into account. Therefore, Fresnel reflection coefficients can be obtained through the summation of infinite series of reflected light.[11] However, since the polarization of s-polarized light is vertical to that of p-polarized light, there is no need to consider the interference between the p- and s-polarized light, then the total reflectance $R_{\rm epi}$ can still be expressed as the mean value of both p- and s-polarized light reflectances, similar to Eq. (5). Consequently, the fitting formulae are summarized as

$$R_{\rm epi} = (r^2_{\rm p,epi} + r^2_{\rm s,epi})/2, \tag{6a}$$

$$r_{\rm p,epi} = \frac{{\rm r}_{1\rm p} + r_{2\rm p}\,{\rm e}^{2{\rm i}\beta_{\rm p}}}{1 + r_{1\rm p} r_{2\rm p}\,{\rm e}^{2{\rm i}\beta_{\rm p}}}, \tag{6b}$$

$$r_{\rm s,epi} = \frac{{\rm r}_{1\rm s} + r_{2\rm s}\,{\rm e}^{2{\rm i}\beta_{\rm s}}}{1 + r_{1\rm s} r_{2\rm s}\,{\rm e}^{2{\rm i}\beta_{\rm s}}}, \tag{6c}$$

where $r_{1\rm p}$ and $r_{1\rm s}$ are Fresnel reflection coefficients at the ambient/epilayer interface for p- and s-polarized light, respectively, and are functions of dielectric function and incident angle; $r_{2\rm p}$ and $r_{2\rm s}$ are Fresnel reflection coefficients at the epilayer/substrate interface for p- and s-polarized light, respectively, and are also functions of dielectric function and incident angle; and $\beta_{\rm p}$ and $\beta_{\rm s}$ are the phase differences for p- and s-polarized light, respectively, and are functions of epilayer thickness (denoted by d), dielectric function, and incident angle.

The details of $r_{1\rm p}$, $r_{1\rm s}$, $r_{2\rm p}$, $r_{2\rm s}$, β_p, and $\beta_{\rm s}$ can be found in Ref. [11], where the complex refractive index (which is the square root of the dielectric function) was used for the case of the absorption film. Therefore, the total reflectance $R_{\rm epi}$ is dependent on dielectric function, incident angle and epilayer thickness. In the following fitting analyses, we adopt the values $\omega_{\rm L\perp} = 970.1$ cm^{-1}, $\omega_{\rm L\parallel} = 965.8$ cm^{-1}, $\omega_{\rm T\perp} = 797.3$ cm^{-1}, $\omega_{\rm T\parallel} = 782.1$ cm^{-1}, $\varepsilon_\infty^{\parallel} = 6.78$, $\varepsilon_\infty^{\perp} = 6.56$, $m^*_{\parallel} = 0.29m_0$, and $m^*_{\perp} = 0.42m_0$ (m_0 is the electron rest mass), according to Refs. [12] and [13].

4. Results and discussion

4.1. Fitting of 4H–SiC substrates and epilayers

Figure 2 shows the experimental and fitted infrared reflectance spectra for the semi-insulating 4H–SiC substrate and n-type 4H–SiC substrates with carrier concentrations of 10^{18} cm^{-1} and 10^{19} cm^{-1}, respectively. A nonlinear least-squares-fit was performed using Eqs. (1)–(5), where $\omega_{\rm p\perp}$, γ, $\Gamma_{\rm L}$, and $\Gamma_{\rm T}$ were set to be adjustable parameters, while $\omega_{\rm L\parallel,\perp}$, $\omega_{\rm T\parallel,\perp}$, $\varepsilon_\infty^{\parallel}$, $\varepsilon_\infty^{\perp}$ were fixed to be constant.

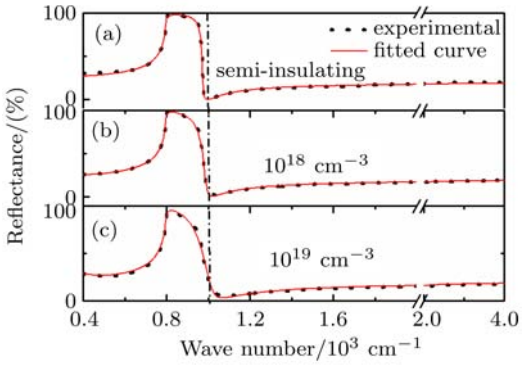


Fig. 2. (colour online) Experimental and fitted infrared reflectance spectra for (a) semi-insulating 4H–SiC substrates (Sample 1) and n-type 4H–SiC substrates with carrier concentrations of (b) 10^{18} cm^{-1} and (c) 10^{19} cm^{-1} (Samples 2 and 3), respectively. The vertical dashed line denotes the shift in minimum reflectance towards high frequency with increasing carrier concentration.

As can be seen in Fig. 2, good fitting results are obtained for both semi-insulating and n-type 4H–SiC substrates. It is clearly shown that two features in the spectra change significantly with increasing carrier concentration. The first feature presents the uptrend of the spectral tail from 400 cm^{-1} to 600 cm^{-1}

with increasing carrier concentration. This is because the higher the carrier concentration, the greater the contribution the Drude term makes to the dielectric function, leading to the uptrend of the spectral tail. The second feature is the distortion of the reststrahlen band ranging from 800 cm^{-1} to 1000 cm^{-1}. This is related mainly to the variations of TO and LO damping constants and plasma frequency with carrier concentration. The TO damping constant primarily influences the maximum reflectance of the reststrahlen band by changing the lattice absorption, whereas the LO damping constant and plasma frequency mainly affect the shape of the reststrahlen band. The maximum reflectance of the reststrahlen band decreases slightly with increasing carrier concentration due to the larger TO damping constant at higher carrier concentration. Besides, as the carrier concentration increases, the rounded edge of the reststrahlen band at about 900 cm^{-1} dips remarkably and the minimum reflectance at around 1000 cm^{-1} is shifted towards high frequency. This reveals that the LO phonon damping constant and the plasma frequency increase with increasing carrier concentration. In the case of higher carrier concentration, the plasma frequency is close to or larger than the pure LO phonon frequency, and then the coupling between them becomes non-negligible. In this case, equation (1) becomes invalid because only the couplings of photon–phonon and photon–carrier are taken into account in the infrared reflectance model used in this study.[8]

Table 1 shows the best-fit parameters of Samples 2 and 3 and their standard errors. The corresponding free-carrier concentrations and mobilities, which were derived from the fit parameters of $\omega_{p\perp}$ and γ by using Eqs. (2) and (3), respectively, are also listed in Table 1 for a comparison with the results from Hall-effect measurements. The carrier concentration is 3.2×10^{18} cm^{-3} and the carrier mobility is 54.4 $cm^2/(V \cdot S)$ for Sample 2, while the carrier concentration is 9.5×10^{18} cm^{-3} and the carrier mobility is 36.8 $cm^2/(V \cdot S)$ for Sample 3. These data are slightly lower than those obtained by Hall measurements. This may be attributed to the fact that some free carriers are trapped in the defects and fail to couple with the infrared photons.[7] The relevant results based on the 4H–SiC semi-insulating substrate are not given because the infrared reflectance technique is inapplicable for the case of low carrier concentration substrates ($< 10^{17}$ cm^{-3}). The details will be discussed in the next section.

Table 1. Best-fit parameters and calculated electrical properties of n-type 4H–SiC substrates. Data in brackets are the estimated standard errors of the best-fit parameters.

		Sample 2	Sample 3
$\omega_{p\perp}/cm^{-1}$		326.34 (1.42)	556.34 (2.26)
γ/cm^{-1}		439.45 (6.78)	649.52 (7.86)
Γ_L/cm^{-1}		7.45 (0.26)	7.68 (0.63)
Γ_T/cm^{-1}		1.51 (0.04)	6.21 (0.23)
N/cm^{-3}	infrared	3.2×10^{18}	9.5×10^{18}
	Hall-effect	5.0×10^{18}	1.05×10^{19}
$\mu/(cm^2/(V \cdot S))$	infrared	54.4	36.8
	Hall-effect	55.4	48.7

The infrared reflectance spectra on several 4H–SiC n-type epilayers with different thicknesses and carrier concentrations were measured. The typical fitted and measured results are presented in Fig. 3. Equations (1), (2), (3), and (6) were used for nonlinear least-squares-fit analyses, where $\omega_{p\perp}$, γ, Γ_L, Γ_T, and d were set to be adjustable parameters, while $\omega_{L\parallel,\perp}$, $\omega_{T\parallel,\perp}$, $\varepsilon_\infty^{\parallel}$, $\varepsilon_\infty^{\perp}$ were fixed to be constant. It is shown that the agreement between the experimental and the calculated profiles is good with the residual sum of squares being 0.06. The best-fit parameters, their standard errors, as well as the calculated electrical properties are summarized in Table 2. The data, obtained by other methods including SEM, Hall measurements, Hg-probe CV, and theoretical formulae, are also listed in the table for comparison. It should be noted that it is difficult to gain accurate electrical properties of epilayers with Hall measurements due to the effects of heavily doped substrates. Hence the carrier concentration and mobility of the epilayer were obtained using Hg-probe CV and the formula in Ref. [14], respectively.

As can be seen in Table 2, epilayer thickness d has a small standard error and accords well with that obtained by SEM measurements. In terms of the calculated electrical properties, $\omega_{p\perp}$ and γ of the substrate exhibit small standard errors, and the substrate carrier concentration and mobility are close to those of the Hall measurements. However, the standard errors of $\omega_{p\perp}$ and γ increase and the discrepancies between the electrical properties obtained by the infrared method and those by other methods become large in the case of low carrier concentration. This can be explained from two perspectives. On the one hand, the epilayer carrier concentration approaches the minimum value (1.0×10^{17} cm^{-3}) detectable by

mid-infrared reflectance measurements, leading to the increased uncertainty of the estimation of the electrical properties of the epilayer. On the other hand, the theoretical value of the mobility is obtained on the assumption that the crystal is perfect. Yet the sample in this experiment includes some surface morphological defects, which can act as the charge recombination centre, thereby severely reducing carrier mobility.

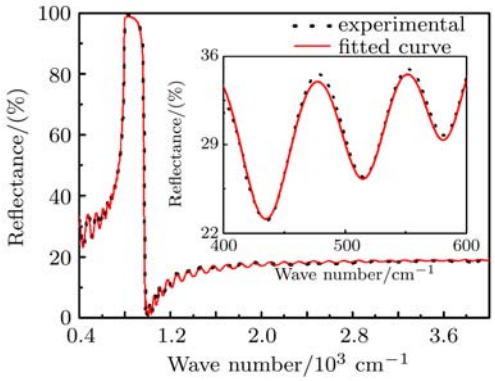


Fig. 3. (colour online) Experimental and fitted infrared reflectance spectra of a thick 4H–SiC n-type epilayer on an n-type substrate. The inset shows the magnified image of the spectra in wave numbers ranging from 400 cm^{-1}–600 cm^{-1}.

Table 2. Best-fit parameters and calculated electrical properties of the 4H–SiC epilayer.

		Epilayer	Substrate
$\omega_{p\perp}$/cm^{-1}		72.98 (9.10)	376.60 (1.15)
γ/cm^{-1}		59.72 (37.98)	447.46 (9.96)
Γ_L/cm^{-1}		3.67 (0.06)	25.27 (1.28)
Γ_T/cm^{-1}		1.42 (0.05)	5.79 (0.71)
N/cm^{-3}	infrared	1.6×10^{17}	4.4×10^{18}
	other methods	8.8×10^{16} [a]	5.0×10^{18} [c]
μ/(cm^2/(V·S))	infrared	400	53.3
	other methods	501[b]	55.4[c]
d/μm	infrared	14.5 (0.005)	–
	SEM	14.4	–

[a] Data from Hg-probe CV. [b] Data from theoretical formula. [c] Data from Hall measurement. Data in brackets are the estimated standard errors of the best-fit parameters.

4.2. Effects of carrier concentration and mobility on spectral profiles

The variations in the theoretical spectral profiles are discussed at different carrier mobilities and concentrations by introducing the error quadratic sum (EQS) parameter. Equations (1)–(5) were used for the theoretical fitting analyses and the fixed parameters were adopted based on the values obtained from the above fitting analyses.

As the total reflectance is dependent only on the dielectric function and incident angle, the spectral profile would be irrelevant to the plasma frequency and damping constant, given that the Drude term in Eq. (1) is ignored. The EQS is defined as the quadratic sum of the difference between two sets of reflectance data; one is extracted from a fitting spectrum obtained using Eq. (1), the other from a fitting spectrum by ignoring the Drude term in Eq. (1). The remaining parameters for the two spectra are set to be the same. It follows that the larger EQS implies that the free carriers make greater contributions to the dielectric function, thus it is more likely to estimate accurate carrier concentration and mobility.

The results are summarized in Figs. 4 and 5. As shown in Fig. 4, the values of the EQS are close to zero and keep constant at different mobilities and a carrier concentration of 2.0×10^{17} cm^{-3} for a spectral region of 400 cm^{-1}–4000 cm^{-1}, revealing that the line shape of the mid-infrared reflectance spectrum is independent of the mobility at a carrier concentration of 10^{17} cm^{-3}. Hence the aforementioned calculated mobility of the epilayer serves only as a reference.

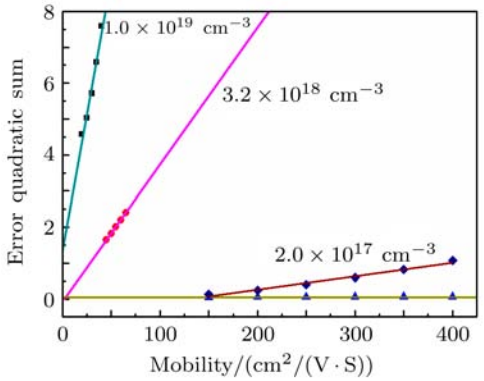


Fig. 4. (colour online) Dependences of the EQS on the mobility for different carrier concentrations and spectral ranges. The mobility ranges used for calculation are 25 cm^2/(V·S)–40 cm^2/(V·S) (■) for 1.0×10^{19} cm^{-3}, 45 cm^2/(V·S)–65 cm^2/(V·S) (●) for 3.2×10^{18} cm^{-3}, and 150 cm^2/(V·S)–400 cm^2/(V·S) (♦ and ▲) for 2.0×10^{17} cm^{-3}, respectively. The spectral ranges are 30 cm^{-1}–4000 cm^{-1} for the data (♦) and 400 cm^{-1}–4000 cm^{-1} for the remaining ones, respectively. The lines are linear fits to the data.

Yet the theoretical results in a spectral range of 30 cm^{-1}–4000 cm^{-1} (indicated by the data (♦) in Fig. 4) show that the accuracy of the calculated mobility at low carrier concentration can be significantly

improved by extending the spectral range to the far-infrared. Thus this is not the fundamental limit of the infrared reflectance measurement, especially considering the fact that far- and mid-infrared reflection spectrometers have been commercialized widely. To confirm the theoretical result, we have also fitted the measured infrared reflectance spectrum of the 4H–SiC epilayer in a spectral range of 30 cm^{-1}–2000 cm^{-1} in Fig. 3 of Ref. [7]. The calculated epilayer carrier concentration and mobility are close to the reported values, indicating the reliability of the above theoretical prediction.

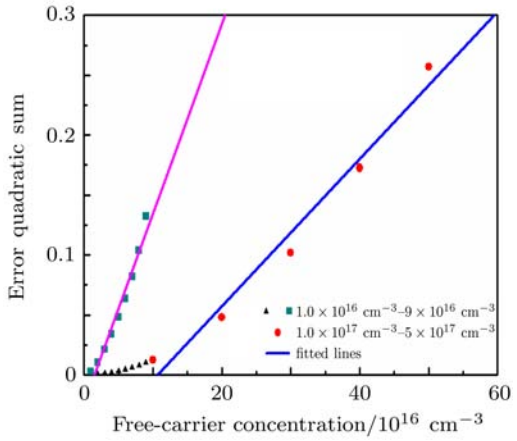


Fig. 5. (colour online) Dependences of the EQS on the carrier concentration with a mobility of 400 $cm^2/(V \cdot S)$. The spectral ranges are 30 cm^{-1}–4000 cm^{-1} for the data (■) and 400 cm^{-1}–4000 cm^{-1} for the data (▲ and ●). The lines are linear fits to the data.

The mobility dependence of the EQS becomes significantly strong when the carrier concentration is enhanced to 10^{18} cm^{-3} and 10^{19} cm^{-3}, owing to the strong coupling between the photons and carriers, as previously discussed. A similar phenomenon was also found in the fitting analysis of the Raman LOPC mode, where the LOPC Raman shift ω_{LOPC} reduced linearly with the increase in plasma damping constant.[15] This may suggest that both infrared reflectance and Raman scattering measurement are more sensitive to the mobility at higher carrier concentration. However, the EQS characterizes the whole infrared spectral profile, while the ω_{LOPC} describes the position of the LOPC mode peak, without involving the peak line width, peak height, and so on.

Figure 5 represents the dependences of the EQS on carrier concentration with a mobility of 400 $cm^2/(V \cdot S)$. It is clearly shown that when the spectral range is from 400 cm^{-3} to 4000 cm^{-3}, the EQS increases linearly with the increase in carrier concentration at a carrier concentration of above 10^{17} cm^{-3}, whereas the EQS becomes quite small when the carrier concentration is below 10^{17} cm^{-3}. This reveals the weak coupling of photon–carrier at low carrier concentration, so the electrical properties of the semi-insulating 4H–SiC substrates and undoped epilayers are unsuited to calculation by the mid-infrared reflectance method. By contrast, the dependence of the EQS on the carrier concentration (below 10^{17} cm^{-3}) becomes significantly strong when a far- through mid-infrared spectral range (30 cm^{-1}–4000 cm^{-1}) is adopted, which is indicated by the data (■) in Fig. 5. It can be concluded that low carrier concentration ($\approx 10^{16}$ cm^{-3}) may be detected by extending the spectral range to the far infrared.

5. Conclusion

In this paper, we measure the mid-infrared reflectance spectra of both 4H–SiC substrates and epilayers, and characterize their carrier concentrations, mobilities, as well as epilayer thicknesses, by curve fitting analyses. The consistency between the thickness data obtained by fitting calculation and those by SEM indicates that the infrared reflectance technique is a reliable thickness measurement method. The introduction of the EQS quantitatively demonstrates that the dependences of the spectral profiles on 4H–SiC electrical properties become significantly strong when the carrier concentration is increased and the spectral range is extended to the far-infrared (30 cm^{-1}–4000 cm^{-1}). These results show that the infrared reflectance technique can be used to accurately determine the carrier concentration and the mobility of both lightly and heavily doped 4H–SiC wafers.

Acknowledgement

The authors would like to thank Dr. Zhou Qun at Tsinghua University for her assistance in the infrared reflectance spectra measurements.

References

[1] Deng X C, Zhang B, Zhang Y R, Wang Y and Li Z J 2011 *Chin. Phys.* B **20** 017304
[2] Sun G S, Liu X F, Wang L, Zhao W S, Yang T, Wu H L, Yan G G, Zhao Y M, Ning J, Zeng Y P and Li J M 2010 *Chin. Phys.* B **19** 088101

[3] Zhao Y M, Sun G S, Li J Y, Liu X F, Wang L, Zhao W S and Li J M 2007 *Chin. Phys. Lett.* **24** 1753
[4] Harima H, Nakashima S and Uemura T 1995 *J. Appl. Phys.* **78** 1996
[5] Sun G S, Liu X F, Wu H L, Yan G G, Dong L, Zheng L, Zhao W S, Wang L, Zeng Y P, Li X G and Wang Z G 2011 *Chin. Phys.* B **20** 033301
[6] Narita K, Hijikata Y, Yaguchi H, Yoshida S and Nakashima S 2004 *Jpn. J. Appl. Phys.* **43** 5151
[7] Oishi S, Hijikata Y, Yaguchi H and Yoshida S 2006 *Jpn. J. Appl. Phys.* **45** L1226
[8] Nakashima S and Harima H 2004 *J. Appl. Phys.* **95** 3541
[9] Born M and Wolf E 1999 *Principles of Optics* 7th edn. (Cambridge: Cambridge University Press) p. 44
[10] Lekner J 1987 *Theory of Reflection* (Dordrecht: Martinus Nijhoff) p. 144
[11] Azzam R M A and Bashara N M 1977 *Ellipsometry and Polarized Light* (New York: North-Holland) p. 358
[12] Tiwald T E, Woollam J A, Zollner S, Christiansen J, Gregory R B, Wetteroth T, Wilson S R and Powell A R 1999 *Phys. Rev.* B **60** 11464
[13] Son N T, Chen W M, Kordina O, Konstantinov A O, Monemar B, Janzen E, Hofman D M, Volm D, Drechsler M and Meyer B K 1995 *Appl. Phys. Lett.* **66** 1074
[14] Pernot J, Contreras S, Camassel J, Robert J L, Zawadzki W, Neyret E and Cioccio L D 2000 *Appl. Phys. Lett.* **77** 4359
[15] Chafai M, Jaouhari A, Torres A, Anton R, Martin E, Jimenez J and Mitchel W C 2001 *J. Appl. Phys.* **90** 5211